A Solutal Interaction Mechanism for the Columnar-to-Equiaxed Transition in Alloy Solidification

M.A. MARTORANO, C. BECKERMANN, and Ch.-A. GANDIN

A multiphase/multiscale model is used to predict the columnar-to-equiaxed transition (CET) during solidification of binary alloys. The model consists of averaged energy and species conservation equations, coupled with nucleation and growth laws for dendritic structures. A new mechanism for the CET is proposed based on solutal interactions between the equiaxed grains and the advancing columnar front—as opposed to the commonly used mechanical blocking criterion. The resulting differences in the CET prediction are demonstrated for cases where a steady state can be assumed, and a revised isotherm velocity (V_T) vs temperature gradient (G) map for the CET is presented. The model is validated by predicting the CET in previously performed unsteady, unidirectional solidification experiments involving Al-Si alloys of three different compositions. Good agreement is obtained between measured and predicted cooling curves. A parametric study is performed to investigate the dependence of the CET position on the nucleation undercooling and the density of nuclei in the equiaxed zone. Nucleation undercoolings are determined that provide the best agreement between measured and calculated CET positions. It is found that for all three alloy compositions, the nucleation undercoolings are very close to the maximum columnar dendrite tip undercoolings, indicating that the origin of the equiaxed grains may not be heterogeneous nucleation, but rather a breakdown or fragmentation of the columnar dendrites.

I. INTRODUCTION

A CHANGE from an outer columnar to an inner equiaxed grain structure is a common occurrence in metal alloy castings, and numerous mechanisms for the columnar-to-equiaxed transition (CET) have been proposed based on experimental evidence.[1] Mathematical modeling of the CET during alloy solidification, however, has had limited success owing to the complex interplay of macroscopic phenomena, such as heat transfer and fluid flow, and microscopic phenomena, such as nucleation and dendritic growth. All previous CET models, as well as the present study, neglect or oversimplify the treatment of melt convection and movement of free equiaxed grains. Usually, equiaxed grains are assumed to nucleate and grow in the constitutionally undercooled liquid ahead of the advancing columnar front, as originally proposed by Winegard and Chalmers.[2] The CET occurs when the advance of the columnar front is blocked by the equiaxed grains.

The CET models can be classified as stochastic or deterministic. Stochastic models aim to follow the nucleation and growth of each individual grain.[3,4,5] No assumptions are made regarding the grain morphology. The evolution of the shape of the envelope of each grain is computed as a function of the local thermal environment. The CET may then be determined based on whether the average final grain shape in a portion of a casting appears more columnar or equiaxed.

The main limitation of stochastic models is related to the large amount of computer resources needed to resolve the large number of grains potentially present in a casting.

Deterministic models of the CET, on the other hand, do not attempt to resolve the nucleation and growth of each grain in a casting. Instead, they rely on averaged quantities and equations that are solved on a macroscopic scale. By tracking the movement of the columnar front and calculating the growth of equiaxed grains in the undercooled liquid in front of it, the CET can still be predicted. A key issue in deterministic models is the selection of a suitable criterion for determining the position where the equiaxed grains block the columnar front and cause the CET. In both stochastic and deterministic models, the nucleation parameters (e.g., nucleation undercooling and number density of nuclei) for the equiaxed grains must be specified.

A. Models of the CET

Hunt[6] proposed the first deterministic model to predict conditions for the CET. A steady-state regime, together with a linear temperature profile characterized by a temperature gradient (G), was assumed for an observer moving with the columnar front. The columnar dendrite tip velocity was taken as a known constant equal to the isotherm velocity. A certain number of equiaxed grains per unit volume (n) was assumed to nucleate instantaneously ahead of the columnar front when the liquid reached an undercooling of $\Delta T_N = T_L(C_0) - T_N$, where $T_L(C_0)$ is the liquidus temperature corresponding to the initial alloy composition (C_0) and T_N is the nucleation temperature. The undercooling of the columnar dendrite tips, $\Delta T_t = T_L(C_0) - T_t$, where T_t is the temperature at the columnar dendrite tips, was calculated from an empirical relation as a function of the isotherm velocity. Using the same relation for the equiaxed grain tip velocity, the volume fraction of equiaxed grains is determined at the position of the columnar front. All undercoolings used for dendrite tip velocity

M.A. MARTORANO, Visiting Professor, Department of Mechanical and Industrial Engineering, The University of Iowa, is on leave from the Department of Metallurgical and Materials Engineering, University of São Paulo, São Paulo-SP, 05508-900, Brazil. C. BECKERMANN, Professor, is with the Department of Mechanical and Industrial Engineering, The University of Iowa, Iowa City, IA 52242-1527. Contact e-mail: becker@engineering.uiowa.edu Ch.-A. GANDIN, Research Fellow, is with the Laboratoire de Science et Génie des Matériaux et de Métallurgie, UMR CNRS-INPL-UHP 7584, Ecole des Mines, F-54042 Nancy, France.
Manuscript received January 6, 2003.

calculations are defined relative to the initial alloy composition. This implies that the liquid surrounding the equiaxed and columnar dendrite tips remains at C_0 and that the solutal boundary layers from neighboring dendrite tips do not interact, even in the mean field. Hunt[6] only accounted for the geometrical interactions due to the impingement of the equiaxed grains. The CET was assumed to occur when the volume fraction of equiaxed grains at the columnar front reached 0.49. This criterion, which will be referred to as "mechanical blocking" in the remainder of this article, was described as arbitrary by Hunt and lacks strong fundamental support.

The final equation derived by Hunt[6] states that the CET occurs or will have occurred when the following condition holds:

$$G < 0.617 \, n^{1/3} \, \Delta T_t \left(1 - \left(\frac{\Delta T_N}{\Delta T_t} \right)^3 \right) \qquad [1]$$

Kim and Grugel[7] and Ledgard and McCartney[8] conducted steady-state solidification experiments in a Bridgeman-type furnace with an approximately constant temperature gradient using Pb-Cu and Al-Si alloys, respectively. It was observed that an increase in the columnar front velocity promoted equiaxed solidification, as predicted by Hunt's[6] equation. Nonetheless, no detailed comparisons were attempted, because neither the density of nuclei nor the nucleation undercooling was known.

Flood and Hunt[9,10] extended Hunt's[6] model to the unsteady regime by solving a one-dimensional energy equation and tracking the position of the columnar front. The solid fraction within the columnar zone was calculated using the so-called truncated Scheil equation.[11] The effect of alloy concentration, number density of equiaxed grains, base heat-transfer coefficient, and pouring temperature on the CET position were examined using the model. No comparisons of model and experimental results were presented, however.

Gäumann et al.[12] and Kurz et al.[13] improved Hunt's model by employing a dendrite growth model that accounts for rapid solidification effects. As in Hunt's model, the initial alloy composition was used in the undercooling to calculate columnar and equiaxed dendrite tip velocities. Consequently, the mechanical blocking criterion had to be adopted to predict the CET. The model was simplified to predict the CET in laser and welding processes, i.e., at large temperature gradients and solidification velocities.[12,13] No experimental comparisons were provided.

Wang and Beckermann[14] proposed a single-domain multiphase/multiscale model to predict the CET in alloy solidification. Energy and species conservation equations were solved for the temperature and solute fields. The species equations included the rejection of solute from the grains into the undercooled liquid, resulting in differences in the Scheil behavior. The solid fraction evolution was calculated in both the columnar and equiaxed zones, based on the coupling of the energy and species equations, and the latent heat evolution was accounted for consistently. The equiaxed grains were assumed to nucleate instantaneously at the liquidus temperature, i.e., the nucleation undercooling was zero. The Lipton-Glicksman-Kurz (LGK) model[15] was used to relate the dendrite growth velocity to the undercooling. For equiaxed growth, the undercooling was based on the local average solute concentration of the undercooled liquid surrounding the dendrites; hence, the solutal interactions between equiaxed grains were taken into account. However, the initial alloy composition was employed to calculate the undercooling at the columnar front; consequently, solutal interactions between the columnar dendrites and the equiaxed grains were neglected. Instead, they used the mechanical blocking criterion of Hunt[6] to determine when the equiaxed grains obstructed the columnar front.

Wang and Beckermann[14] performed a parametric study to examine the effects of a base heat transfer coefficient, alloy composition, and pouring superheat on the CET in directionally solidified alloys. Predicted and measured CET positions for Sn-Pb[16] and Al-Cu[17] alloys differed by less than 20 pct. However, since the nucleation undercooling was taken as zero, this agreement was only achieved by artificially adjusting the density of the equiaxed grain nuclei, n, in the simulations. For the Al-Cu alloys, a grain density equal to 10^5 m^{-3} was adopted. This density corresponds to a final equiaxed grain size of approximately 13 mm, which is much larger than the measured size of 3.1 mm.[17] Furthermore, predicted and measured cooling curves were not compared in detail.

Gandin and Rappaz proposed a stochastic model that gives a direct two-dimensional simulated macrograph of the grain structure.[5] Based on the coupling between a cellular-automaton (CA) technique and a finite-element (FE) method (CAFE), the CAFE model only accounted for the interaction of the heat flow with the grain structure. It was used to simulate the CET in a directionally solidified Al-7 wt pct Si ingot. Adjustment of the nucleation parameters was carried out in order to reach the best agreement with both the position of the CET and the recalescence in the equiaxed zone. Good agreement was achieved, except for the grain size at the top part of the equiaxed zone. This disagreement was later attributed to the need to account for sedimentation of equiaxed grains[18] and the three-dimensionality of the grain structure.[19]

Gandin[20] presented a comprehensive micro-macroscopic one-dimensional heat transfer model of columnar growth in directional solidification. The model was used to simulate experiments of Al-Si alloys with Si contents ranging from 3 to 11 pct and identical thermal conditions.[21] The model results indicated that the measured CET occurred at a position where the columnar front velocity was a maximum and the temperature gradient in the liquid ahead of the columnar front was almost zero. Hence, Gandin suggested that Hunt's[6] model could be employed to explain the measured position of the CET by using the maximum columnar dendrite tip undercooling as the nucleation undercooling for equiaxed grains in Eq. [1]. Based on this observation, Gandin proposed that the CET was a result of a breakdown of the columnar dendritic front. The breakdown occurs due to a mechanism originally suggested by Jackson et al.,[22] wherein changes in the columnar front velocity create dendrite fragments from which equiaxed grains can originate. Upon growth, these grains eventually block the columnar front.

B. Experiments on the CET in Directional Solidification of Binary Alloys

Numerous experiments have been conducted to study the CET in various solidification processes. Here, we focus on experiments where the heat flow was essentially unidirectional

and the alloy was a simple binary system, namely, Al-Cu,[17,23,24] Al-Si,[21] Sn-Pb,[16,24] Cu-Sn,[25,26] Pb-Sn,[27] and Al-Mg.[28] In these experiments, the position of the CET in the solidified samples was studied as a function of process variables, including pouring superheat, addition of inoculants, alloy composition, heat extraction rate, and average cooling rate. In all cases, the experimental apparatus basically consisted of a thermally insulating sleeve resting on a metallic base, through which the heat was extracted. Since the samples were cooled from the bottom, thermally driven natural convection on a large scale was minimized; however, solutally driven natural convection can be important for the alloys where the lighter component is rejected (*e.g.*, Cu-Sn and Pb-Sn), if the stabilizing thermal gradient is too small. Furthermore, it cannot be ruled out that settling of equiaxed grains had some influence on the CET in the experiments.

Ziv and Weinberg[17] used Hunt's[6] model to calculate the maximum temperature gradient necessary for the CET in one of their experiments with Al-3 pct Cu alloys. Despite reasonable agreement between the predicted and measured temperature gradients, the calculations involved a number of approximations that cast some doubt on the accuracy of the comparison.

Suri *et al.*[23] performed experiments of the CET in Al-4.5 pct Cu alloys subject to different pouring temperatures and heat extraction conditions. Using a one-dimensional heat-transfer model, the temperature gradient and the liquidus isotherm velocity (V_T) at the moment of the CET were calculated. They obtained the following empirical inequality to describe conditions for the CET:[23]

$$G < 0.74 V_T^{0.64} \qquad [2]$$

Despite the similarity between Eq. [2] and Eq. [1] from Hunt's[6] model, no comparison was attempted.

Gandin[21] carried out experiments of the CET in directional solidification of Al-Si alloys with Si contents ranging from 3 to 11 pct and identical thermal conditions. Convection associated with the pouring of the liquid metal was suppressed by using a thin aluminum nitride base to seal the insulated cylindrical sleeve at the bottom and keeping the Al-Si melt in the furnace for a long time. After homogenization of the melt temperature, solidification was initiated by removing the furnace from the mold and raising a water-cooled copper chill to touch the bottom of the high thermal conductivity aluminum nitride base. Cooling curves recorded by seven thermocouples located every 20 mm from the bottom of the casting were compared with predictions of a one-dimensional model,[20] suggesting that heat transfer in the solidifying metal was by conduction only. Measured CET positions were similar for all alloy compositions, indicating a weak effect of the Si content. Further conclusions drawn from the simulations were already provided in the previous section.

Martorano and Capocchi[25,26] presented detailed experimental results of the CET in Cu-8 pct Sn alloys subject to different cooling and inoculation conditions. No comparisons with mathematical models of the CET were made, however.

Ares and Schvezov[27] studied the effect of the average cooling rate and alloy composition on the CET in directionally solidified Pb-Sn alloys. The columnar front position and velocity, as well as the temperature gradient, were calculated from experimental cooling curves. The results showed a correlation similar to that given by Hunt's model[6] between the columnar front velocity and the temperature gradient at the moment of the CET. Nevertheless, owing to certain approximations made and uncertainties regarding the density of equiaxed grain nuclei and the nucleation undercooling, only qualitative agreement could be claimed.

Vandyoussefi and Greer[28] carried out directional solidification experiments using an Al-4.5 pct Mg alloy in a Bridgman furnace. The grain shape and size were measured for several refiner addition levels, showing good agreement with simulations from the CAFE model.[5] The CET was observed to be gradual in both measurements and simulations and was reasonably well predicted by Hunt's[6] model. Because the experiments were conducted in a high isotherm velocity and high temperature gradient regime, the CET was sensitive to the density of equiaxed grain nuclei, as predicted by Hunt's model.

Very recently, Siqueira *et al.*[24] performed CET experiments involving Al-Cu and Sn-Pb alloys by changing the composition, melt superheat, and heat extraction rate at the bottom. The temperature gradient at the liquidus isotherm and the velocity of this isotherm during the experiments were determined using a one-dimensional heat transfer model that does not account for the undercooling at the columnar front. They found that a CET criterion based only on either the liquidus isotherm velocity or the temperature gradient ahead of the liquidus isotherm was not supported by their experimental data. Instead, the CET appeared to occur when the cooling rate at the liquidus isotherm decreased below a critical value that was independent of the solute content of the alloy. It should be noted, however, that there can be considerable differences between the temperature gradient or isotherm velocity at the columnar front and those at the liquidus temperature, and that previous studies[20] took the columnar front undercooling into account and evaluated those quantities at the columnar front. The empirical criterion for the CET proposed by Suri *et al.*[23] (Eq. [2]) was verified in only two out of five experiments. No direct comparison with Hunt's model[6] (Eq. [1]) was presented.

C. *Objectives of the Present Study*

The main objective of the present study is to propose a new mechanism for the CET. This new mechanism (and the undercooling for the nucleation of equiaxed grains) is included in a modified version of the deterministic multi-phase/multiscale model of Wang and Beckermann.[14] The modified model is then used to predict the CET measured in the directional solidification experiments of Gandin[21] involving Al-Si alloys. The proposed CET mechanism is based on the presence of solutal interactions between the columnar front and the equiaxed grains. It not only eliminates the need for the mechanical blocking criterion in deterministic models, but also results in different CET predictions under certain conditions. Extensive comparisons of the present model with previous models and experiments, as well as parametric studies, are carried out. In the comparisons with the experiments, which involve three different alloy compositions, the grain densities obtained from the measured final equiaxed grain sizes are used in the model. The nucleation undercooling resulting in the

best agreement between measured and predicted CET positions and cooling curves is determined for each experiment in order to validate the model.

II. MATHEMATICAL MODEL

A. *Governing Equations*

The governing equations are based directly on the model of Wang and Beckermann.[14] Therefore, the equations are only briefly described, followed by detailed comments on the new features of the present model.

In an attempt to separate the various length scales present in dendritic solidification, Wang and Beckermann[14] defined three phases within a representative elementary volume (REV): solid (s), interdendritic liquid (d), and extradendritic liquid (l). The volume fractions of the three phases are denoted by ε_s, ε_d, and ε_l, respectively, such that $\varepsilon_s + \varepsilon_d + \varepsilon_l = 1$. As illustrated in Figure 1, the inter- and extradendritic liquids are separated by an imaginary dendrite or grain envelope that is a smooth surface extending around the dendrite tips. The envelope surface area per unit volume in the REV is denoted by S_e. The grain envelope volume fraction is defined as $\varepsilon_g = \varepsilon_s + \varepsilon_d = 1 - \varepsilon_l$. It is this grain fraction on which the traditional mechanical blocking criterion for the CET is based (*i.e.*, the CET occurs when $\varepsilon_g = 0.49$ in Hunt's[6] criterion). Finally, an internal solid volume fraction can be defined as $\varepsilon_{si} = \varepsilon_s/\varepsilon_g$. When the internal solid fraction is unity, the equiaxed grains are said to be globulitic (*i.e.*, fully solid globules).

The REV in Figure 1 is assumed to be isothermal at a temperature of T and average composition of C_0. The interdendritic liquid is associated with the relatively small length scale of the spaces between the dendrite arms inside the envelope and is assumed to be solutally well mixed at the
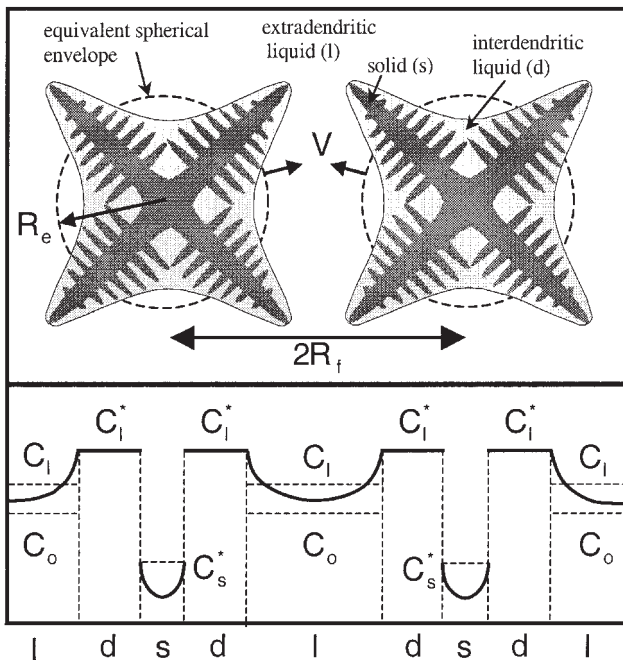

Fig. 1—Schematic illustration of two dendrite envelopes and the local solute concentration profiles in a representative elementary volume of average composition C_0 and uniform temperature T.

liquidus concentration (C_l^*) given by the phase diagram at the temperature T. The extradendritic liquid, on the other hand, is associated with the larger length scale of the distance between the primary dendrite arms or equiaxed grains and can, generally, not be taken to be solutally well mixed. When its average solute concentration (C_l) is below C_l^*, the extradendritic liquid is undercooled. It is this undercooling that primarily drives the dendritic growth. Due to solute rejection by the growing dendrites/grains into the finite extradendritic liquid, C_l can become greater than C_0. The presence of a solute profile in the solid in Figure 1 simply reflects the fact that the mass diffusivity of the solid (D_s) is typically much smaller than that of the liquid (D_l). This results in incomplete solute diffusion in the solid, even though the length scale for diffusion is the same as that for the interdendritic liquid. In fact, back-diffusion in the solid is completely neglected in the present study.

In deriving the governing equations, melt flow, movement of solid, and macroscopic solute diffusion are neglected. This implies that the local mixture solute concentration (in a REV) remains at the initial alloy composition. Furthermore, it is assumed that the specific heats (c_p) and the densities (ζ) of the phases are equal and constant. The thermal conductivity (κ) of the mixture in a REV is calculated from $\kappa = \varepsilon_s \kappa_s + (\varepsilon_d + \varepsilon_l)\kappa_l$. Then, for the one-dimensional system (in z) considered in the present study, the volume-averaged conservation equations for energy, interdendritic liquid solute, and extradendritic liquid solute can be written, respectively, as[14]

$$\rho c_P \frac{\partial T}{\partial t} = \frac{\partial}{\partial z}\left(\kappa \frac{\partial T}{\partial z}\right) + \rho L \frac{\partial \varepsilon_s}{\partial t} \qquad [3]$$

$$(1 - k)\, C_l^* \frac{\partial \varepsilon_s}{\partial t} = \varepsilon_d \frac{\partial C_l^*}{\partial t} + S_e \frac{D_l}{\delta_e}(C_l^* - C_l) \qquad [4]$$

$$\frac{\partial(\varepsilon_l C_l)}{\partial t} = C_l^* \frac{\partial \varepsilon_l}{\partial t} + S_e \frac{D_l}{\delta_e}(C_l^* - C_l) \qquad [5]$$

where L is the latent heat and k is the solute partition coefficient. The last term in Eqs. [4] and [5] accounts for diffusion of solute from the growing dendrites/grains into the undercooled extradendritic liquid. The diffusion length (δ_e) in this term is discussed in greater detail subsequently and in the Appendix. In the absence of extradendritic liquid ($\varepsilon_l = 0$), this term vanishes and Eq. [4] reduces to the differential form of the Scheil equation. The previous equations are coupled by the liquidus line of a binary equilibrium phase diagram, *i.e.*,

$$C_l^* = \frac{(T - T_f)}{m_l} \qquad [6]$$

where T_f is the melting point of the pure metal, and m_l is the liquidus line slope. Then, Eq. [4] can be solved for the solid fraction, ε_s, and Eq. [5] provides the average solute concentration in the extradendritic liquid, C_l.

The following equation is used to calculate the grain (or extradendritic liquid) volume fraction:

$$\frac{\partial \varepsilon_g}{\partial t} = -\frac{\partial \varepsilon_l}{\partial t} = S_e V \qquad [7]$$

where V is the dendrite tip velocity. This velocity is obtained from the growth model originally proposed by Lipton et al.[15] (LGK)

$$V = \frac{4\sigma^* D_l m_l (k-1) C_1^*}{\Gamma} \left(Iv^{-1}(\Omega) \right)^2 \quad [8]$$

where $\sigma^* \approx 1/(4\pi^2)$ is the stability constant, Γ is the Gibbs–Thomson coefficient, and Iv^{-1} is the inverse of the Ivantsov function, which can be approximated by the following equation:[14]

$$Iv^{-1}(\Omega) = 0.4567 \left(\frac{\Omega}{1-\Omega} \right)^{1.195} \quad [9]$$

The dimensionless undercooling (Ω) is defined as

$$\Omega = \frac{C_l^* - C_l}{C_l^*(1-k)} \quad [10]$$

Note that in Eq. [10] the undercooling is defined relative to the *average* solute concentration in the undercooled extradendritic liquid, C_l. Hunt,[6] Gäumann et al.,[12] and Kurz et al.[13] used instead the initial alloy composition, C_0, to determine the undercooling for dendrite growth. Wang and Beckermann[14] adopted C_l for equiaxed growth, but C_0 for columnar growth. Here, C_l is used for both equiaxed and columnar growth. This seemingly minor difference constitutes the main new feature of the present model. It is discussed in more detail in Section II–C and is shown to eliminate the need for a mechanical blocking criterion for predicting the CET.

B. Supplementary Relations for Equiaxed and Columnar Growth

While the equations of the preceding section are equally valid for columnar and equiaxed growth, the envelope area per unit volume (S_e) and the envelope diffusion length, δ_e, depend on the type of growth. These two quantities govern solute rejection into the undercooled extradendritic liquid between the dendrite envelopes. This solute diffusion is dissimilar in equiaxed and columnar growth, primarily because the spacing between the envelopes can be of a different magnitude. As shown in Figure 1, the characteristic spacing between the envelopes is denoted by $2R_f$ and extends from center to center. The spacing between the equiaxed envelopes is governed by the equiaxed grain density, whereas the columnar envelope spacing is determined by the primary dendrite arm spacing (λ_1). The following expressions are used to obtain a first-order estimate of the characteristic half-spacing (R_f) in the two types of growth:

$$\text{equiaxed: } R_f = \left(\frac{3}{4\pi n} \right)^{1/3} \quad \text{columnar: } R_f = \lambda_1/2 \quad [11]$$

Since the uncertainties in n and λ_1 are often large, more exact expressions that take into account the detailed arrangement of the dendrite envelopes in the REV are not considered here. The evolution of n and λ_1 must, in general, be obtained from separate models or empirical relations. For simplicity, it is assumed that n nuclei appear instantaneously at a melt

undercooling equal to ΔT_N. More complex nucleation models could be easily implemented. In the present study, the actual values for n, ΔT_N, and λ_1 are either determined in a parametric study or estimated from the microstructure observed in experiments, as explained in greater detail subsequently.

Another issue in modeling the solute diffusion into the extradendritic liquid is the shape of the dendrite envelopes. Wang and Beckermann[14] assumed a spherical shape for the equiaxed grain envelopes and a cylindrical shape for the columnar envelopes. Considering the uncertainties in the envelope geometry, a simpler model is employed here where the basic envelope shape is spherical for both columnar and equiaxed growth. While this approximation may seem inadequate for columnar growth, it was verified to result in only minor differences to the Wang and Beckermann[14] model.

Assuming a spherical envelope shape, the following expression can be written for the envelope area per unit volume:[14]

$$S_e = \frac{3(1-\varepsilon_l)^{\frac{2}{3}}}{R_f} \quad [12]$$

Note that Eq. [12] does not account for impingement of the envelopes as the extradendritic liquid fraction approaches zero. This is a good approximation when the dendrite envelopes of neighboring grains or primary branches do not bridge because secondary phases (e.g., eutectic) form between them. More importantly, the undercooling of the extradendritic liquid usually vanishes well before the envelopes impinge. Then, further solidification occurs in a Scheil mode, and the envelope area and diffusion length play no role in the present model.

The envelope diffusion length is calculated as a function of the envelope Peclet number, $Pe = VR_e/D_l$, from

$$\frac{\delta_e}{R_e} = \frac{3R_e e^{Pe}}{(R_f^3 - R_e^3)} \int_{R_e}^{R_f} \left(\int_{R_e}^{r} \frac{e^{-Pe\frac{r'}{R_e}}}{r'^2} dr' \right) r^2 dr \quad [13]$$

where the instantaneous envelope radius (R_e) is given by

$$\frac{R_e}{R_f} = (1-\varepsilon_l)^{\frac{1}{3}} \quad [14]$$

Because Eq. [13] differs slightly from the one used by Wang and Beckermann,[14] its derivation is provided in the Appendix. The Appendix also provides a closed-form analytical solution to Eq. [13].

In summary, with the assumption of spherical envelopes for both types of growth, the present set of model equations is identical for columnar and equiaxed growth, except for the equation used to calculate the characteristic envelope half-spacing (Eq. [11]). This results in some simplification in the implementation of the model in a numerical code. The prominent role played by R_f is further discussed in the next section.

C. The CET Mechanism

The main new feature of the present model is that both the equiaxed and columnar dendrite growth velocities are a function of a solutal undercooling proportional to the

difference between the local liquidus concentration and the local average solute concentration in the extradendritic liquid (Eq. [10]). At least for columnar growth, all other models[5,6,14,12,13,20] used the initial alloy composition C_0 instead of C_l in the dimensionless undercooling, *i.e.*,

$$\Omega = \frac{C_l^* - C_0}{C_l^* (1 - k)} \qquad [15]$$

For the previous models, this implies that for a given columnar dendrite tip temperature, the tip velocity is the same regardless of the presence of equiaxed grains growing ahead of the columnar front. It also implies that a mechanical blocking criterion is needed to "stop" the columnar front and simulate the CET.

The CET mechanism operating in the present model is schematically illustrated in Figure 2. The directional solidification system shown in Figure 2 is characterized by a certain temperature gradient. Equiaxed grains nucleate at T_N in undercooled liquid of a concentration $C_l = C_0$ behind the liquidus isotherm ($T_L(C_0)$). The equiaxed grains growing in front of the columnar dendrites reject solute into the extradendritic liquid, which causes C_l to increase over C_0 as the columnar front is approached. Deep inside the columnar zone, the melt is no longer undercooled and $C_l = C_l^*$. The present model produces a continuous variation in the concentration of the extradendritic liquid from C_0 to C_l^* in the direction of decreasing temperature. If the solute rejection by the equiaxed grains is sufficiently strong, the undercooling, $T_L - T = m_l (C_l - C_l^*)$, which is proportional to the distance between the C_l^* and C_l curves in Figure 2, will have already vanished ahead of the columnar tips. This not only
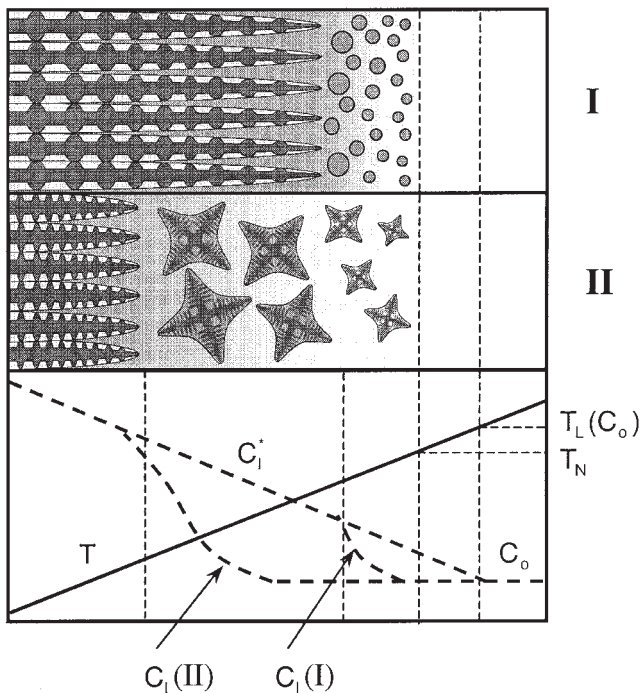

C_l(II)   C_l(I)

Fig. 2—Schematic illustration of the solutal interactions between the columnar dendrites and equiaxed grains during the CET. Case I is for a high equiaxed grain density and case II is for a low density; the temperature gradient and nucleation undercooling are the same in both cases.

stops the equiaxed dendritic growth, but also the columnar growth, and a CET results.

The two different cases shown in Figure 2 illustrate why the present model can result in different CET predictions compared to previous deterministic models where the CET is assumed to always occur when the equiaxed grain volume fraction (ε_g) at the columnar front is equal to 0.49. Both cases are characterized by the same temperature gradient, alloy composition, and equiaxed grain nucleation temperature, but different columnar front velocities. In case I, the equiaxed grain density is relatively large, as would be the case if an inoculant (grain refiner) had been used, and the equiaxed grains remain more or less globulitic. In case II, the grain density is comparatively small and the equiaxed grains become highly dendritic. Since the grain density determines the characteristic envelope spacing in equiaxed growth (Eq. [11]), it is useful to compare this spacing to the primary dendrite arm spacing in columnar growth. Case I corresponds to a situation where the spacing between the equiaxed grains is of the same order of magnitude as or smaller than the primary dendrite arm spacing, *i.e.*, $n^{-1/3} \leq O(\lambda_1)$. In case II, on the other hand, $n^{-1/3} \gg O(\lambda_1)$.

In case I, the large equiaxed grain density causes the envelope area per unit volume to increase sharply as soon as the liquid fraction decreases from unity (Eq. [12]). According to Eq. [5], a large S_e value results in a small solutal undercooling, because the last term in this equation must remain finite. Therefore, C_l approaches C_l^* in a small distance behind the nucleation isotherm. In other words, the large number of globulitic grains in case I reject a large amount of solute into the surrounding liquid, causing a rapid reduction of the solutal undercooling ahead of the columnar front. Hence, in case I, the CET can occur when the equiaxed grain volume fraction ($\varepsilon_g = 1 - \varepsilon_l$) is still much lower than 0.49. As a consequence, the CET occurs at a lower columnar front velocity compared to case II (for the same G and T_N values), as indicated in Figure 2 by the higher columnar tip temperature.

In case II, the small equiaxed grain density causes S_e to remain small even when the grain fraction is relatively large. According to Eq. [5], this causes C_l to remain at C_0 behind the nucleation isotherm for a distance much longer than that in case I. Only when the equiaxed grain envelopes have enough time to grow to a size where the extradendritic liquid fraction becomes very small, will C_l approach C_l^*. Hence, in case II, the CET can occur when the equiaxed grain volume fraction is greater than 0.49. It is shown subsequently that, for a small grain density, the CET occurs after a very rapid increase in the volume fraction of equiaxed grains. Therefore, it is not meaningful to associate a specific equiaxed grain fraction with the CET in case II, since 0.49 works as well as any value between approximately 0.2 and 0.9. Consequently, for a small grain density, the present solutal blocking mechanism provides predictions of the CET similar to those given by the mechanical blocking criterion.

D. *Numerical Solution*

The system of 13 equations (Eqs. [3] through [14] plus the equation $\varepsilon_d = 1 - \varepsilon_l - \varepsilon_s$) corresponds to the thirteen unknowns T, V, ε_s, ε_l, ε_d, R_f, R_e, Iv, Ω, S_e, δ_e, C_l^*, and C_l.

A numerical solution is given by solving the system of six equations (Eq. [3] through [8]) for the six unknowns T, V, ε_s, ε_l, C_l^*, and C_l, from which the remaining unknowns can be directly calculated. The conservation equations are discretized by the implicit control volume method[29] and are solved by a segregated scheme. First, the system of algebraic equations resulting from the discretized form of Eq. [3] is solved using the Tri-Diagonal Matrix Algorithm (TDMA) algorithm.[29] For the first iteration, the phase-change rate $(\partial \varepsilon_s / \partial t)$ is estimated from the previous time step. Second, the discretized forms of Eqs. [4] through [8] are solved at each volume element iteratively. Since the latter system of equations does not contain spatial derivatives, convergence can be achieved for each volume element separately. Next, the first system (Eq. [3]) is solved again, and the process is repeated until convergence. This segregated solution procedure has an advantage over the simultaneous solution of all equations. For the volume elements undergoing phase change, more iterations are usually necessary. With the segregated scheme, only the second system of equations for that specific volume has to be iterated further. On the other hand, with a simultaneous solution scheme, all equations for all volume elements would have to be iterated further. The disadvantage of the segregated scheme, however, is that outer iterations are needed for complete convergence of all equations.

Knowing the columnar front velocity, the front position is updated from

$$z_{\text{col}}^{t+\Delta t} = z_{\text{col}}^t + V_{\text{col}}^{t+\Delta t} \Delta t \qquad [16]$$

The knowledge of the columnar front position is solely needed in order to decide which equation to use to calculate R_f (Eq. [11]). Because $V_{\text{col}}^{t+\Delta t}$ sensitively depends on the concentrations C_l^* and C_l at the new time $t + \Delta t$ (Eq. [8]), Eq. [16] must be solved iteratively together with the other model equations. Because C_l and the volume fractions can vary quite rapidly close to the columnar front when the CET is approached (Figure 2), a very fine grid is necessary to accurately resolve these gradients in the numerical solution. Since the strong gradients are limited to a region close to the columnar front, a local mesh refinement procedure was implemented, where the three control volumes closest to the columnar front are subdivided into smaller volumes. When the columnar front

moves from one control volume to another, a new volume is refined and a refined volume is unrefined.

III. THE CET IN QUASI-STEADY SOLIDIFICATION

The present model is examined in more detail by performing quasi-steady simulations, where a constant temperature gradient and a constant isotherm velocity are imposed in a directional (one-dimensional) solidification system. This allows for a direct comparison of the present model with Hunt's CET criterion. Quasi-steady solidification is achieved in the simulations by disregarding the energy equation (Eq. [3]) and instead imposing the following linear temperature profile:

$$T(z,t) = T_L - (GV_T)t + Gz \qquad [17]$$

where T_L is the liquidus temperature corresponding to the initial alloy composition. All simulations in this section are performed for a representative Al-3 pct Cu alloy, whose properties are listed in Table I.

A. Solutal Interactions

The solutal interactions are quantitatively examined in the following section for purely equiaxed growth. Simulations are performed for a cooling rate of $G \times V_T = 0.005$ K/s, a vanishing nucleation undercooling, and for a single control volume (with $z = 0$ in Eq. [17]), such that all dependent variables are a function of time only. Results are presented for four different equiaxed nuclei densities: $n = 2.4 \times 10^5$, 8.8×10^6, 2.4×10^8, and 2.4×10^{11} m^{-3}. According to Eq. [11], these nuclei densities give the following characteristic half-spacings for the equiaxed grains, respectively: $R_f = 10$, 3, 1, and 0.1 mm. Figure 3(a) shows the temporal evolution of the equiaxed grain volume fraction in the four cases, together with the temperature variation. Figure 3(b) shows the corresponding variations in the liquid solute concentrations, and Figure 3(c) shows the variations in the internal solid volume fraction.

It is useful to first focus on the curves corresponding to the largest equiaxed grain half-spacing, $R_f = 10$ mm. It can be seen from Figure 3(a) that grain growth is initially very

Table I.   Material Properties and Microstructural Parameters Used in the Various Simulations

| Property	Al-3 pct Cu	Al-3 pct Si	Al-7 pct Si	Al-11 pct Si
D_l (m$^2 \cdot$s^{-1})	5×10^{-9}	7.0×10^{-9}	6.4×10^{-9}	5.8×10^{-9}
κ_s (W$\cdot$m$^{-1} \cdot$K^{-1})	—	$253 - 0.110\,T$	$233 - 0.110\,T$	$191 - 0.0671\,T$
κ_l (W$\cdot$m$^{-1} \cdot$K^{-1})	—	$41.5 - 0.0312\,T$	$36.5 + 0.028\,T$	$27.6 + 0.0333\,T$
L (J$\cdot$kg^{-1})	—	387.4×10^3	387.4×10^3	387.4×10^3
c_p (J$\cdot$kg$^{-1} \cdot$K^{-1})	—	1126	1126	1126
ρ (kg$\cdot$m^{-3})	—	2452	2452	2452
m_l (K$\cdot$pct wt^{-1})	-3.37	-6.0	-6.5	-7.0
k (–)	0.17	0.12	0.13	0.14
Γ (m$\cdot$K)	2.41×10^{-7}	1.96×10^{-7}	1.96×10^{-7}	1.96×10^{-7}
T_L(K)	923	913	891	863
T_{eut}(K)	821	850	850	850
R_f (mm)	—	4.0	2.5	5.0
n (m^{-3})	—	3.7×10^6	1.5×10^7	1.9×10^6
λ_1 (mm)	—	1.5	1.5	1.5
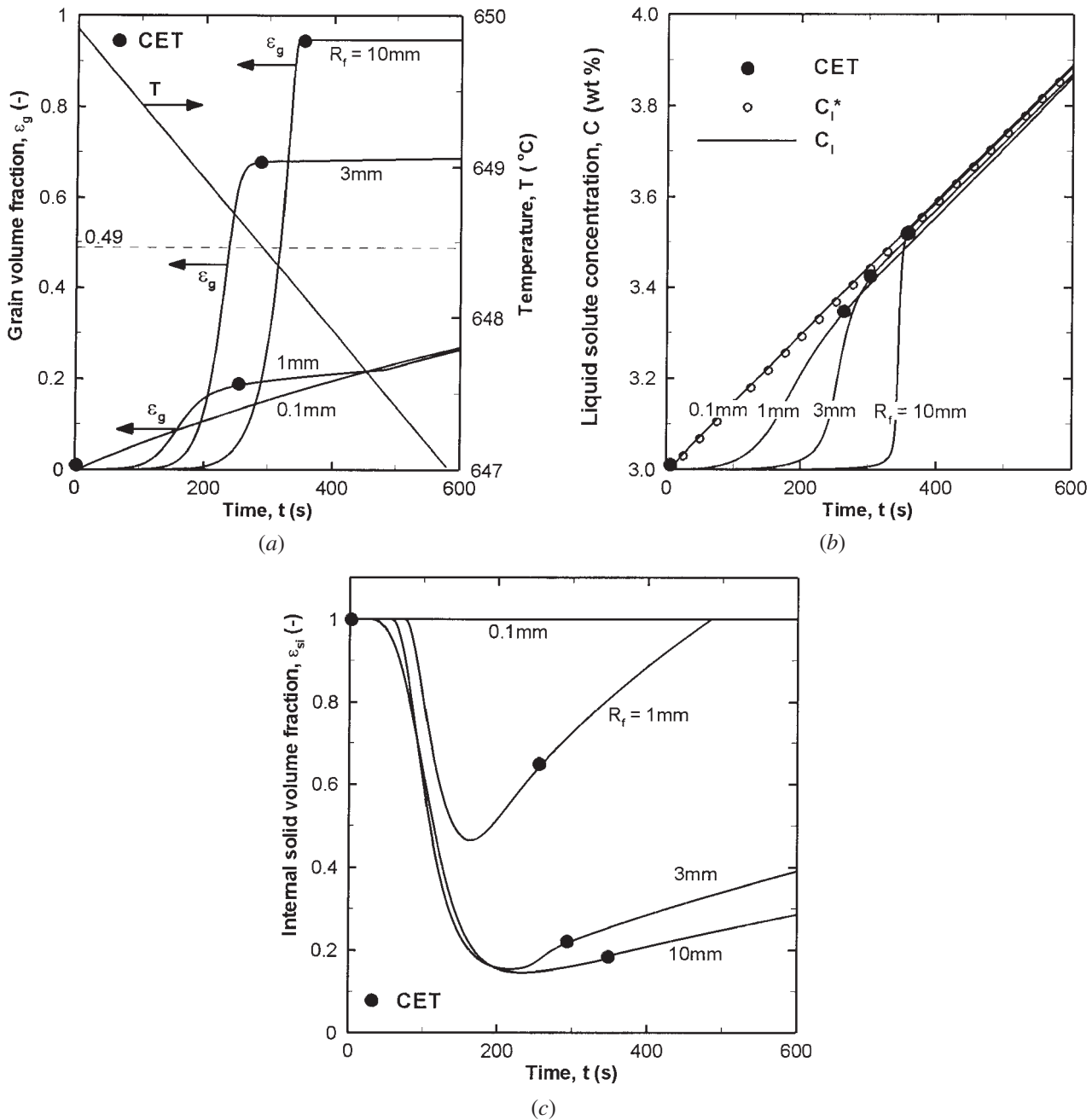
Fig. 3—Model predictions for a single control volume containing equiaxed grains of an Al-3 pct Cu alloy cooled at a constant rate ($R = -0.005$ K/s) for different equiaxed grain half-spacings, R_f, and a zero nucleation undercooling: evolution of (a) the grain volume fraction and the temperature, (b) the liquid solute concentrations, and (c) the internal solid volume fraction.

slow (until about 200 seconds), which can be attributed to the small values of the envelope area concentration (S_e) in Eq. [7]; note that $S_e \sim 1/R_f$, according to Eq. [12]. Figure 3(b) shows that during this period, very little solute is rejected into the extradendritic liquid (because of the small values of S_e in the last term of Eq. [5]), and the extradendritic liquid concentration, C_l, remains at C_0. Figure 3(c) indicates that during the first 200 seconds, the internal solid fraction, ε_{si}, decreases from unity (for the initial nuclei) to about 0.15, implying that the grains become highly dendritic. Starting at 200 seconds, the grains undergo a period of rapid growth until the grain fraction reaches a value of about 0.95 at 350 seconds (Figure 3(a)). This rapid increase

in ε_g can be attributed to S_e in Eq. [7] and to the solutal undercooling in Eq. [8] for the dendrite tip velocity simultaneously reaching larger values. In response to the decreasing extradendritic liquid fraction ($\varepsilon_l = 1 - \varepsilon_g$), the concentration C_l increases very rapidly to C_l^* at around 350 seconds (Figure 3(b)), i.e., the undercooling dissipates within a few seconds. The time when the solutal undercooling reaches a negligibly small value and dendritic grain growth ceases is marked as a solid circle in Figure 3. This circle is labeled "CET" only to indicate that if columnar grains were present, they would stop growing too. Beyond 350 seconds, solidification is in a Scheil mode. In essence, this case with $R_f = 10$ mm corresponds closely to the

physical situation that underlies the model of Hunt,[6] in that the solutal interactions are negligibly small and the growth undercooling is equal to $C_l^* - C_0$, until very close to the CET. This fact, coupled with the rapid increase in ε_g close to the CET, means that a mechanical blocking criterion with a critical grain fraction of 0.49 would have given a CET prediction similar to that from the present model. In the $R_f = 10$ mm case, any blocking fraction between about 0.2 and 0.95 would give CET predictions within about 50 seconds.

A similar result is obtained for the case with $R_f = 3$ mm, except that the undercooling dissipates earlier due to the somewhat larger values of S_e at early times. Also, the maximum equiaxed grain fraction, corresponding to the time when the undercooling vanishes, is only about 0.7. Nonetheless, the fact that C_l remains at C_0 during most of the growth period, coupled with the rapid increase in ε_g close to the point marked as CET, again implies that Hunt's[6] model would give a similar prediction.

The situation is different for the case with $R_f = 1$ mm. In this case, the equiaxed grain spacing is small enough to cause solutal interactions even when the grain volume fraction is still small. It can be seen from Figure 3(a) that the grain growth occurs more gradually, with a significant increase in ε_g occurring between 100 and 250 seconds. The extradendritic liquid concentration increases gradually throughout that period (Figure 3(b)). This means that using $C_l^* - C_0$ as the solutal undercooling in the growth law of Eq. [8], as done by Hunt,[6] would significantly overestimate the dendrite tip velocity for about half of the total growth period. Since in the present model the undercooling is based on $C_l^* - C_l$ the solutal interactions result in a natural decrease in the dendrite tip velocity. Note that at the time when the undercooling vanishes (at about 250 seconds), the grain fraction is only 0.2, implying that, for relatively small spacings between equiaxed grains, the dendrite growth velocities approach zero well before the grains fill the entire space. Even though the equiaxed grain volume fraction is only 0.2, columnar grains would not "overgrow" the equiaxed grains, because the undercooling necessary for dendrite growth is zero. Most importantly, the use of a mechanical blocking fraction of 0.49 would have given very different results for the CET in this case. Finally, it is interesting to note that due to solutal interactions, the internal solid fraction for the $R_f = 1$ mm case never reaches 0.15 as observed in the previous two cases, but has a minimum of about 0.5 (Figure 3(c)). In fact, ε_{si} increases back to unity at later times.

The curves in Figure 3 for $R_f = 0.1$ mm correspond to a highly grain refined alloy. It can be seen that the interactions between the equiaxed grains are so strong that the melt is solutally well mixed from the very beginning of growth (i.e., $C_l = C_l^*$, Figure 3(b)), and the point marked as CET is close to $t = 0$ (i.e., a purely equiaxed structure would be observed in a directionally solidified ingot). Furthermore, the internal solid fraction remains at unity (Figure 3(c)), implying that, as expected for a highly grain-refined alloy, the grains are globulitic. With $\varepsilon_{si} = 1$, the grain fraction ε_g is equal to the solid fraction ε_s. Hence, the increase of ε_g in Figure 3(a) is not due to dendritic growth, but simply reflects solidification of the solid globules in a Scheil mode.

B. *The CET Map*

For the case of quasi-steady, directional solidification, a CET transition map can be established through simulations by varying the imposed temperature gradient and isotherm velocity until a transition from columnar to equiaxed growth occurs. Figure 4 presents such a map for an Al-3 pct Cu alloy (Table I), assuming a representative value for the nucleation undercooling of $\Delta T_N = 0.75$ K. Transition curves are shown for equiaxed nuclei densities of 10^5 and 10^9 m^{-3}, essentially covering the two extreme cases discussed previously in connection with Figure 3. The straight dashed line with a negative slope added in Figure 4 shows the range of temperature gradients and isotherm velocities that corresponds to the constant cooling rate ($G \times V_T = 0.005$ K/s) used for Figure 3. Combinations of V_T and G to the left-hand side of the transition curves give an equiaxed structure and, to the right-hand side, a columnar structure.

In Figure 4, the CET transition map established using the present model is compared to Hunt's[6] model (Eq. [1]). It must be noted that Hunt used the following empirical equation, instead of Eq. [8], to relate the dendrite tip undercooling to the tip velocity for both equiaxed and columnar growth:

$$V = \frac{3 \times 10^{-4}}{C_0} \Delta T_t^2 \qquad [18]$$

$$\Delta T_t = m_l(C_0 - C_l^*) \qquad [19]$$

The resulting original CET map by Hunt is plotted as a gray line in Figure 4. For verification purposes, the computer code for the present model was modified to mimic Hunt's model by using the previous dendrite tip growth model and implementing the mechanical blocking criterion. The
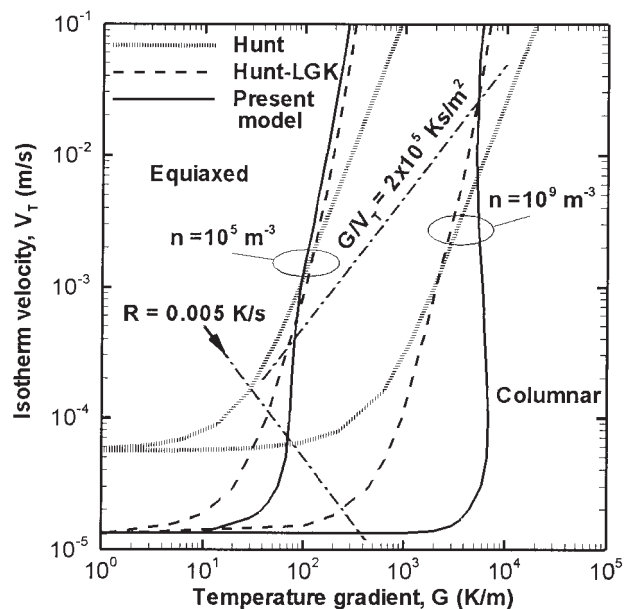
Fig. 4—Columnar-to-equiaxed transition map for steady-state directional solidification of an Al-3 pct Cu alloy for a nucleation undercooling equal to 0.75 K and for two different equiaxed nuclei densities. Results are shown for the present model (solid lines), Hunt's[6] original model (gray lines), and Hunt's model modified to use the same dendrite tip growth model (LGK) as the present model (dashed lines).

numerical results were found to be identical to the analytical predictions given by Eq. [1], thus establishing confidence in the present calculations. In order to achieve a more meaningful comparison with the present model, Hunt's model was modified by replacing Eq. [18] with the current dendrite tip growth model given by Eq. [8], but calculating the undercooling from Eq. [15] (*i.e.*, the undercooling is still measured relative to C_0, as in Eq. [19]) and using the mechanical blocking criterion. This modified model of Hunt, denoted as Hunt-LGK, is plotted as a dashed line in Figure 4.

Figure 4 shows that the choice of a dendrite growth model has a strong effect on the CET map. Comparing the original Hunt and the Hunt-LGK curves, it can be seen that for a low G value, the CET shifts to a lower V_T value by about a factor of 5 when using the LGK dendrite growth model. Note that both the growth law and the nucleation undercooling control the position of the horizontal portion of the transition curve. For higher G values, the slopes of the transition curves are larger with the LGK model than those with Eq. [18]. These differences were already noted by Gäumann *et al.*[12]

Comparing now the CET curves resulting from the present model to the Hunt-LGK curves, it can be seen from Figure 4 that they converge to the same lines in the limit of G approaching zero (*i.e.*, the horizontal portion of the curves). This can be expected, because in the low-G regime, the CET is independent of the nuclei density and is controlled by the isotherm velocity only. The two models also give very similar results for the CET for a G/V_T ratio smaller than about 2×10^5 Ks/m^2 (dashed straight line in Figure 4 with a positive slope). There are, however, important differences at intermediate temperature gradients and isotherm velocities. For the same V_T value, the present model results in the CET shifting to a higher G value compared to the Hunt-LGK model. In other words, for the same G value, the CET shifts to a lower V_T value. The differences are smaller for the lower equiaxed nuclei density ($n = 10^5$ m^{-3}). This can be expected, because for low n values, the solutal interactions are negligible until very close to the time when the CET occurs, as discussed in the preceding subsection. For the higher equiaxed nuclei density ($n = 10^9$ m^{-3}), on the other hand, the solutal interactions cause significant differences and the shift in G can be by up to one order of magnitude.

IV. COMPARISON WITH DIRECTIONAL SOLIDIFICATION EXPERIMENTS

The purpose of this section is to validate the present model using data from directional solidification experiments. As reviewed in Section I, such direct comparisons have been quite rare or ambiguous in the literature, and most researchers have assumed quasi-steady conditions in the experiments in order to apply steady-state CET maps. The experiments chosen for the present comparison are those of Gandin[21] involving three different Al-Si alloys. They are simulated using the fully transient version of the present model, including the energy equation.

A. *Experimental Conditions*

Experiments were performed with Al-Si alloys with initial compositions of 3, 7, and 11 wt pct silicon, resulting in three simulation cases. The corresponding material properties and microstructural parameters used in the simulations are summarized in Table I. A detailed discussion of the properties can be found in the article by Gandin.[20] The measured average equiaxed grain half-spacings are $R_f = 4$, 2.5, and 5 mm for the 3, 7, and 11 pct Si experiments, respectively. The sensitivity of the CET to the equiaxed grain density is examined in greater detail subsequently.

The boundary and initial conditions, domain size, number of unrefined volume elements in the mesh, and time step adopted in each of the three simulations are provided in Table II. As mentioned previously, the three volumes near the columnar front location were refined, each being divided into 41 new volumes. The heat flux at the upper boundary of the domain was obtained by matching measured and predicted cooling curves.[20] The temperature at the lower boundary was prescribed as a function of time in the simulation, by using the experimental cooling curve at the lowest position ($z = 20$ mm).[20] A uniform temperature, determined from the experiments, was used as the initial condition. The variation of the initial melt superheat for the three alloys is shown graphically in Figure 5. It can be seen that the initial superheat increases from about 125 K for the Al-3 pct Si alloy to almost 180 K for the Al-11 pct Si alloy. As will be seen from the measured temperatures presented subsequently, the cooling conditions were approximately the same for all three experiments.

Figure 5 also shows the measured CET positions for the three alloy compositions. The CET occurred at essentially the same vertical position between 110 and 120 mm from the bottom of the samples in all three experiments. Photographs of the macrostructure are provided in the original reference.[20]

B. *Cooling Curves*

The measured and predicted cooling curves are compared in Figures 6 through 8 for each of the three experiments. With the nuclei density determined from the equiaxed grain size measurements (Table I), the only free parameter in the simulations is the nucleation undercooling, ΔT_N. As described in detail in Section IV–C, the nucleation undercoolings were determined through an iterative procedure where ΔT_N was varied until the measured and predicted CET positions agreed.

Figures 6(a), 7(a), and 8(a) show the comparisons of the cooling curves over most of the duration of the 3, 7, and 11 pct Si experiments, respectively. The liquidus and eutectic temperatures for each alloy composition are also indicated. Overall, excellent agreement is obtained.

Table II. Boundary and Initial Conditions, Domain Size, Time Step, and Number of Mesh Volumes Used in the Simulations of the Al-Si Experiments

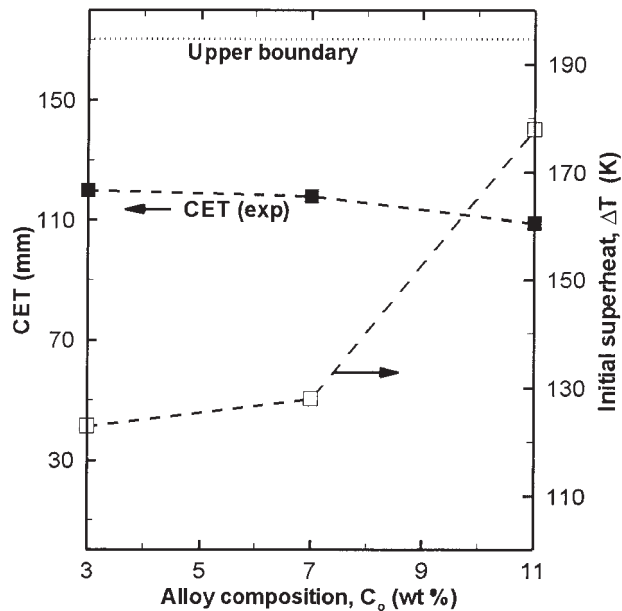| Condition	Al-3 pct Si	Al-7 pct Si	Al-11 pct Si
Upper boundary condition (W/m^2)	4000 for $t \leq 900$ s		5000 for $t \leq 1250$ s
	0 for $t > 900$ s		0 for $t > 1250$ s
Lower boundary condition		Measured $T(t)$ for $z = 20$ mm	
Initial temperature (K)	1036	1019	1041
Domain size (mm)	150	150	150
Time step (s)	5×10^{-3}	5×10^{-3}	5×10^{-3}
Mesh volumes	200	200	200

Fig. 5—Variation of the measured CET position and initial melt superheat with alloy composition in the Al-Si experiments of Gandin.[20]

Figures 6(b), 7(b), and 8(b) show close-ups of the cooling curves around the time of the CET. In each case, the upper horizontal axis is at the liquidus temperature ($T_L(C_0)$). The variation of the calculated columnar dendrite tip temperature (T_t) is also shown; as expected, the columnar tip undercooling ($\Delta T_t = T_L(C_0) - T_t$) vanishes abruptly at the CET, implying no further growth. Even at the magnification of Figures 6(b), 7(b), and 8(b), the agreement between the measured and predicted temperatures is good.

It can be seen that the recalescences or temperature plateaus shown by the thermocouples in the equiaxed zone (at $z = 120$ and 140 mm) are predicted to within better than 0.5 K in all three cases. Gandin[20] simulated the Al-7 pct Si experiment without considering equiaxed grain nucleation and growth. The temperatures predicted by Gandin continually decrease until they reach the columnar tip temperature. In the present simulations, the recalescences/plateaus occur above the columnar tip temperature (if one extends the T_t line horizontally), in accordance with the experimental results. The measured cooling curves for the Al-11 pct Si case (Figure 8(b)) show a more pronounced recalescence at $z = 120$ and 140 mm than predicted. In addition, the predicted cooling curves show seemingly unphysical oscillations during the recalescences/plateaus. Through extensive additional numerical studies it was verified that these oscillations are *not* due to numerical errors, *i.e.*, they are independent of the grid and time step size. It was found that they are inherent to the model, being caused by the assumption of instantaneous nucleation of equiaxed grains. Modeling nucleation as a continuous event taking place over a small range of temperatures would have eliminated the oscillations and have also given better agreement for the recalescence in Figure 8(b). For the Al-3 pct Si experiment (Figure 6(b)), the measured cooling curves show similar oscillations during the plateau, as predicted; however, these oscillations were due to the noise associated with the temperature
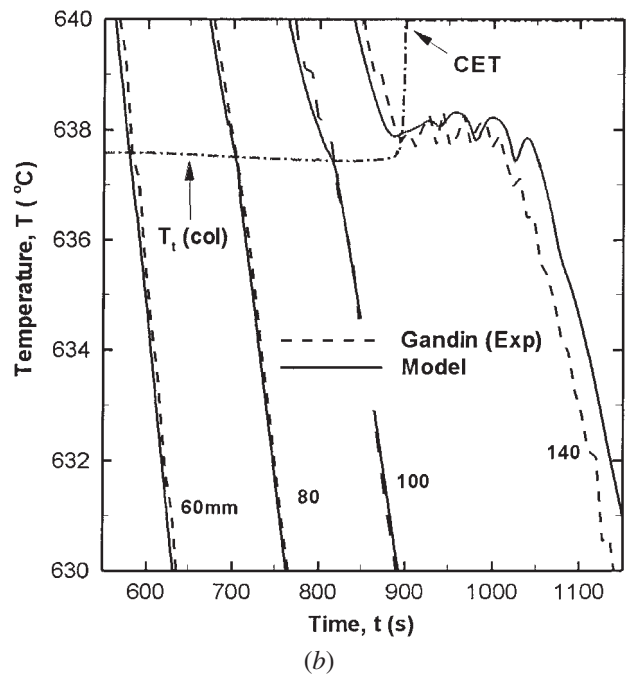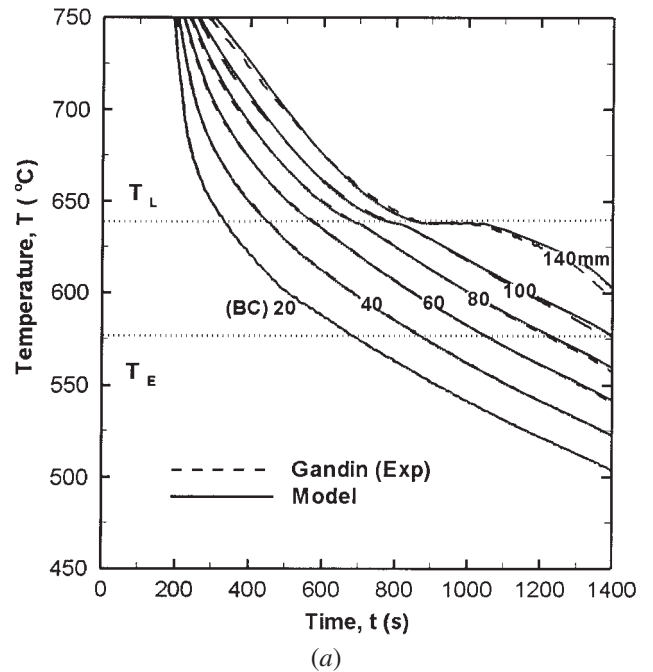

(a)

(b)

Fig. 6—Comparison of measured and predicted cooling curves in the Al-3 pct Si experiment: (a) overall view and (b) enlargement below the liquidus temperature around the CET time.

measurements. Determining the necessary parameters for a continuous nucleation model was outside the scope of this study.

The equiaxed grain nucleation undercoolings, determined by matching the predicted and measured CET positions (additional detail provided in Section IV–C), place the predicted recalescences/plateaus at the correct temperature level. The sensitivity of the temperature level of the recalescences to the nucleation undercooling is illustrated for the Al-7 pct Si experiment in Figure 7(c). In Figure 7(c), the experiment was resimulated using a vanishing equiaxed nucleation
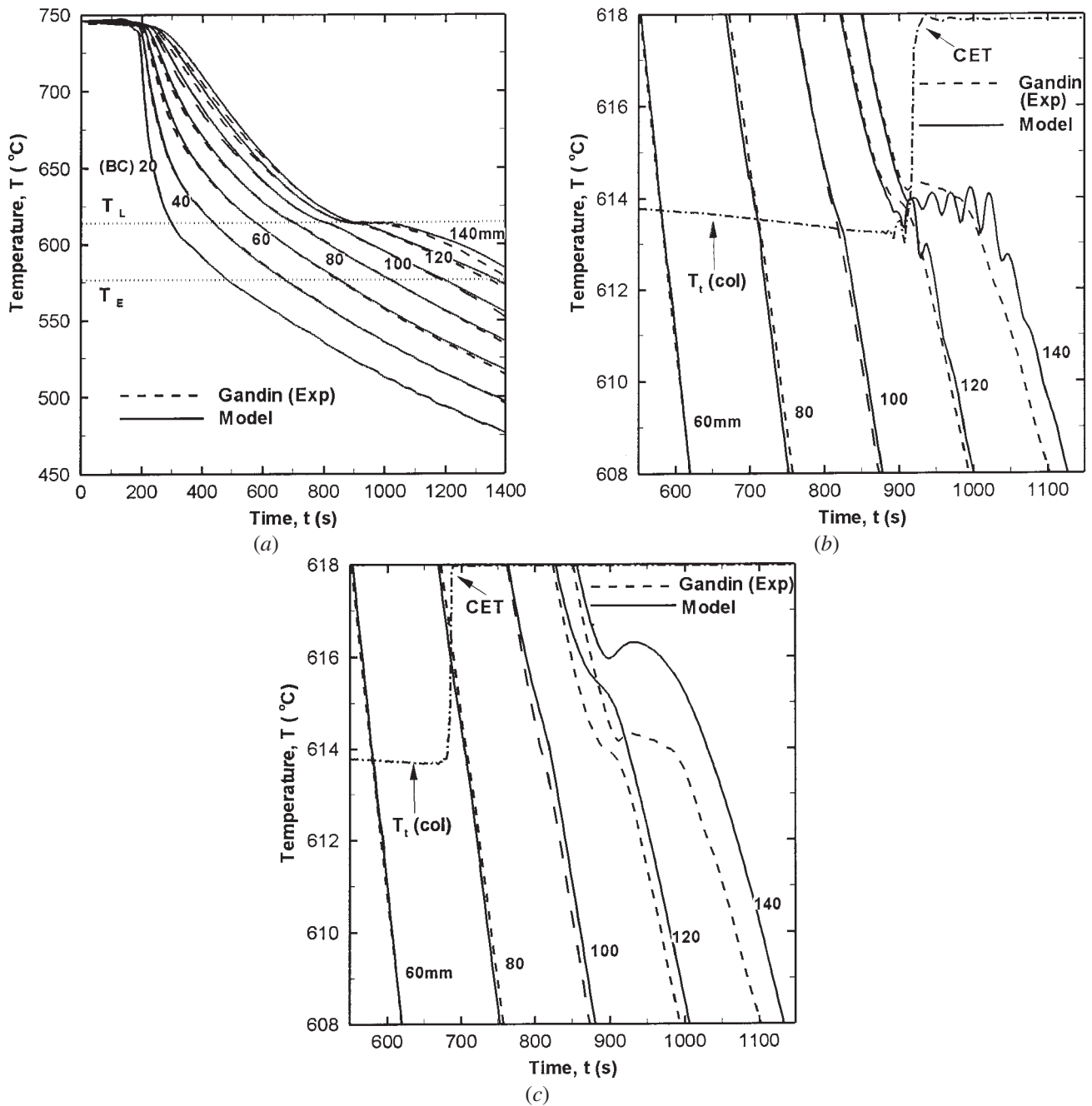
Fig. 7—Comparison of measured and predicted cooling curves in the Al-7 pct Si experiment: (*a*) overall view, (*b*) enlargement below the liquidus temperature around the CET time, and (*c*) simulation results for a vanishing nucleation undercooling (0 K).

undercooling ($\Delta T_N = 0$ K), instead of the one determined by matching the measured and predicted CET positions ($\Delta T_N = 4.7$ K; Figure 7(b)). It can be seen from the columnar tip temperature variation in Figure 7(c) that with $\Delta T_N = 0$ K, the CET occurs almost 250 seconds earlier, implying a much lower CET position than that measured. Also, the recalescences occur at a temperature level about 2 K higher than that measured. This comparison, therefore, shows that there is only one nucleation undercooling that gives good agreement between the measurements and predictions for both the CET and the recalescense temperature level.

In conclusion, the predicted temperatures agree with the measured cooling curves to an extent which one could not

realistically expect to be much better. The inclusion of equiaxed grain nucleation and growth in the model captures the recalescences or temperature plateaus observed in the equiaxed zones. The accurate simulation of the thermal history of the experiments now allows for a detailed examination of the nucleation and growth phenomena leading to the CET.

C. *Determination of the Equiaxed Grain Nucleation Undercooling*

The nuclei density and nucleation undercooling for the equiaxed grains are the main uncertainty in any prediction of the CET. Therefore, a parametric study was undertaken
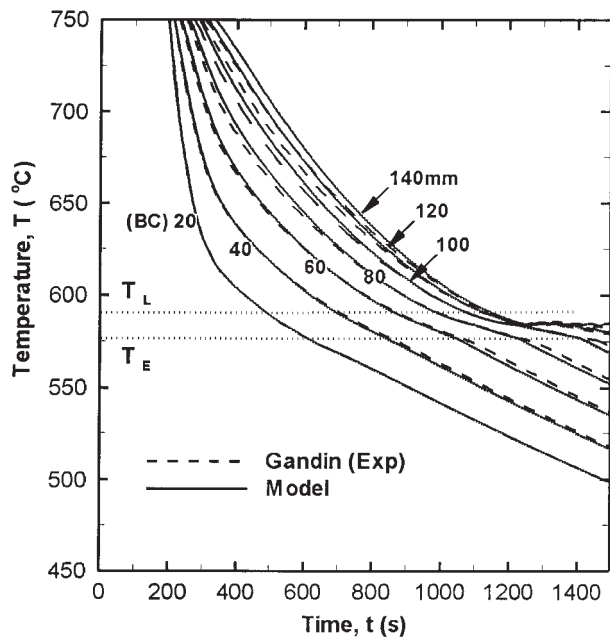
(a)
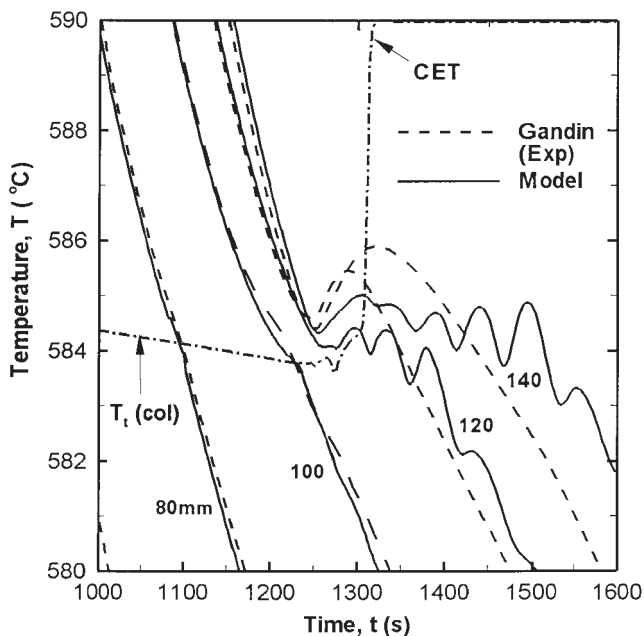
(b)

Fig. 8—Comparison of measured and predicted cooling curves in the Al-11 pct Si experiment: (a) overall view and (b) enlargement below the liquidus temperature around the CET time.
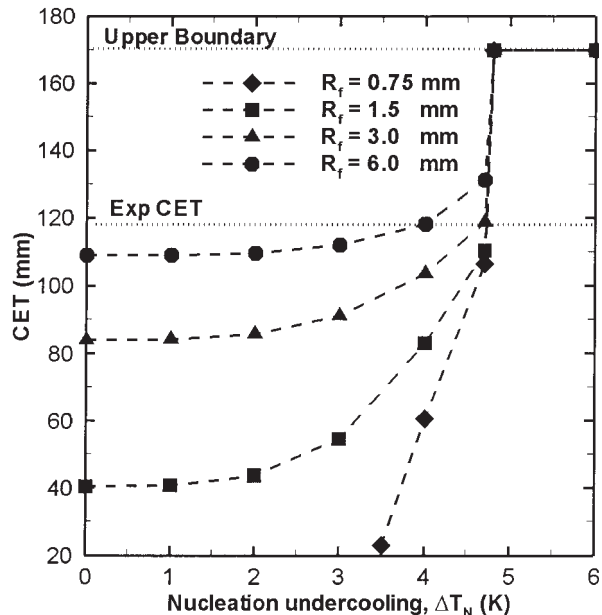

Fig. 9—Predicted variation of the CET position with nucleation undercooling for various equiaxed grain half-spacings in the Al-7 pct Si experiment; the measured CET position and the upper boundary domain are indicated as dotted lines.

to investigate the sensitivity of the CET predictions to n and ΔT_N. The nuclei density is used only in Eq. [11] for calculating the half-spacing between the equiaxed grains. Since R_f is actually measured in the experiments, it is more meaningful to vary R_f (for the equiaxed grains) directly. By using the measured R_f value, the nucleation undercooling that results in a match of the measured and predicted CET positions can then be determined.

Figure 9 shows the predicted CET position as a function of the nucleation undercooling for equiaxed grain half-spacings ranging from 0.75 to 6.0 mm. The measured CET

position and the upper domain boundary are indicated as dotted lines. This graph corresponds to the conditions of the Al-7 pct Si experiment; the graphs for the other two experiments are qualitatively similar. As expected, with increasing ΔT_N values, the CET position moves up the casting, implying a longer columnar zone. However, the increase is very small up to about $\Delta T_N = 2$ K. The CET position also moves up with increasing R_f values, as expected. There is a critical nucleation undercooling of about 4.7 K, above which the structure becomes fully columnar, regardless of R_f. This can be understood by realizing that the maximum columnar dendrite undercooling is about 4.7 K for the Al-7 pct Si experiment (Figure 7(b)); obviously, equiaxed grains could not nucleate ahead of the columnar front if ΔT_N were greater than the maximum ΔT_t (unless the thermal gradient in the liquid becomes negative). For the same reason, the CET becomes independent of R_f (or n) for vanishing (positive) thermal gradients in the CET map of Figure 4. Referring back to Figure 4, it can be seen that in this low-G regime, the CET occurs when V_T exceeds a certain value (which depends on ΔT_N).

Interestingly, Figure 9 shows that the CET measured in the Al-7 pct Si experiment coincides with the point where the curves for all R_f values converge at the critical ΔT_N of 4.7 K. This means that using a nucleation undercooling slightly smaller than 4.7 K produces the "correct" CET in the simulation, regardless of R_f (within the range considered realistic, based on the grain-size measurements). Such a ΔT_N value also produced the good agreement between the measured and predicted recalescences in Figure 7. The same is qualitatively true for the other two experiments. Figure 10 plots the nucleation undercooling, determined as described previously by matching the measured and predicted CET positions, as a function of the alloy composition for all three experiments. It can be seen that ΔT_N increases from about
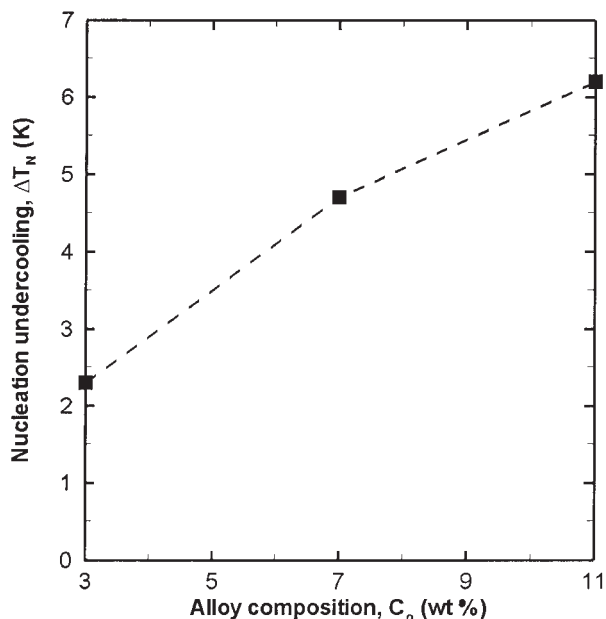
Fig. 10—Variation of the predicted nucleation undercooling with alloy composition in the Al-Si experiments.

2.6 K for the Al-3 pct Si alloy to 5.9 K for the Al-11 pct Si alloy. In each case, ΔT_N was found to be slightly smaller than, but approximately equal to, the maximum columnar dendrite tip undercooling (Figures 6(b), 7(b), and 8(b)).

D. Transition Profiles

The CET in the present directional solidification cases can be better understood by examining the volume fraction and concentration profiles across the transition zone. Figure 11 shows the predicted profiles of solid fraction, grain fraction, extradendritic liquid concentration, and interdendritic liquid concentration ($C_l^* =$ the concentration at the liquidus) profiles for the Al-7 pct Si case over a distance of 20 mm around the position of the CET; the columnar front position is indicated as a thin vertical line. The profiles for the other two alloys are qualitatively similar. The sequence of profiles provided in Figures 11(a) through (d) corresponds to four different times, starting when both columnar and equiaxed grains are growing unimpeded (at 912 seconds) and ending when the columnar front velocity, V_{col}, vanishes and the CET occurs (at 926 seconds). The total time period from the first appearance of equiaxed grains to the blocking of the columnar front is only about 14 seconds long. During this time, the columnar front moves by less than 2 mm, indicating that the grain structure changes relatively abruptly from columnar to equiaxed. This is in complete agreement with the experimental macrographs of Gandin[20] and should be contrasted to situations where the CET is more gradual.[28]

Figure 11(a) corresponds to the time (912 seconds) when equiaxed and columnar grains are growing without significant interaction. Ahead of the columnar front, the melt concentration is uniformly at C_0, indicating that the equiaxed grains have not yet rejected enough solute to slow the columnar front ($V_{col} = 0.15$ mm/s). The melt undercooling vanishes within a very short distance (<1 mm) upon entering the columnar mush,

and $C_l = C_l^*$ further inside the mush. Within this short distance, dendritic growth causes the grain fraction to increase rapidly from 0.4 to about 0.75, whereas the solid fraction increases abruptly to about 0.1. This jump in ε_s has motivated previous researchers to use the so-called truncated Scheil approach[9,10,20] when modeling the solid fraction evolution within the columnar zone in the presence of columnar tip undercooling. In the present study, the sharp transitions in the volume fractions and liquid concentration at the columnar front are a direct result of the model equations. The full numerical resolution of these gradients necessitates, however, the use of local mesh refinement, as described earlier.

Figure 11(b) shows that 6 seconds later (at 918 seconds), the columnar front velocity has already decreased to 0.05 mm/s, which can be attributed to solutal interactions with the equiaxed grains. The interactions cause the solutal undercooling ($C_l^* - C_l$) at the columnar front to decrease. The equiaxed grain fraction at the columnar front has increased to about 0.8. This growth of the equiaxed grains takes place over a distance of only about 3 mm ahead of the columnar front. The solid fraction in the equiaxed zone is also increasing, and the jump in ε_s at the columnar front is less pronounced. Two seconds later (at 920 seconds; Figure 11(c)) the profiles have evolved to a state where the CET is imminent. The solutal undercooling at the columnar front has almost vanished, and the columnar front velocity is down to 0.003 mm/s. Finally, at 926 seconds (Figure 11(d)), the columnar front velocity has decreased to virtually zero, indicating that the CET has already occurred. Fully grown equiaxed grains now exist in a layer about 3 mm thick ahead of the columnar front. Inside this layer, the solutal undercooling is close to zero. Ahead of the layer, the undercooling sharply increases, the solid fraction experiences a jump, and new equiaxed grains keep nucleating.

E. The CET Map

A CET map for an Al-7 pct Si alloy with $n = 1.5 \times 10^7$ m^{-3} ($R_f = 2.5$ mm) is shown in Figure 12. Transition lines are shown for nucleation undercoolings of 5, 3, and 0 K. For each case, predictions are provided for the present model (solid lines) and the Hunt-LGK model (dashed lines). Superimposed on the map is the solidification path for the Al-7 pct Si experiment of Gandin. The isotherm velocities and temperature gradients ahead of the columnar front were determined from the simulation of the experiment. Isotherm velocity and temperature gradient combinations at columnar front positions ranging from 20 to 120 mm, in 20 mm intervals, are indicated on the pathline as solid circles.

It can be seen that the CET position of about 118 mm measured in this experiment indeed corresponds to a nucleation undercooling of 4.7 K (i.e., slightly below the 5 K transition line) in the map. In accordance with the previous discussion, the CET occurs in the low-G regime of the map, where the transition lines are horizontal and the predictions of the present model coincide with those of the Hunt-LGK model. It should be noted that if the nucleation undercooling were only slightly lower, for example, 3 K, considerable differences in the predicted CET position between the two models would be present (40 and 90 mm for the present model and the Hunt-LGK model, respectively). In the limit of a vanishing nucleation undercooling, the present model
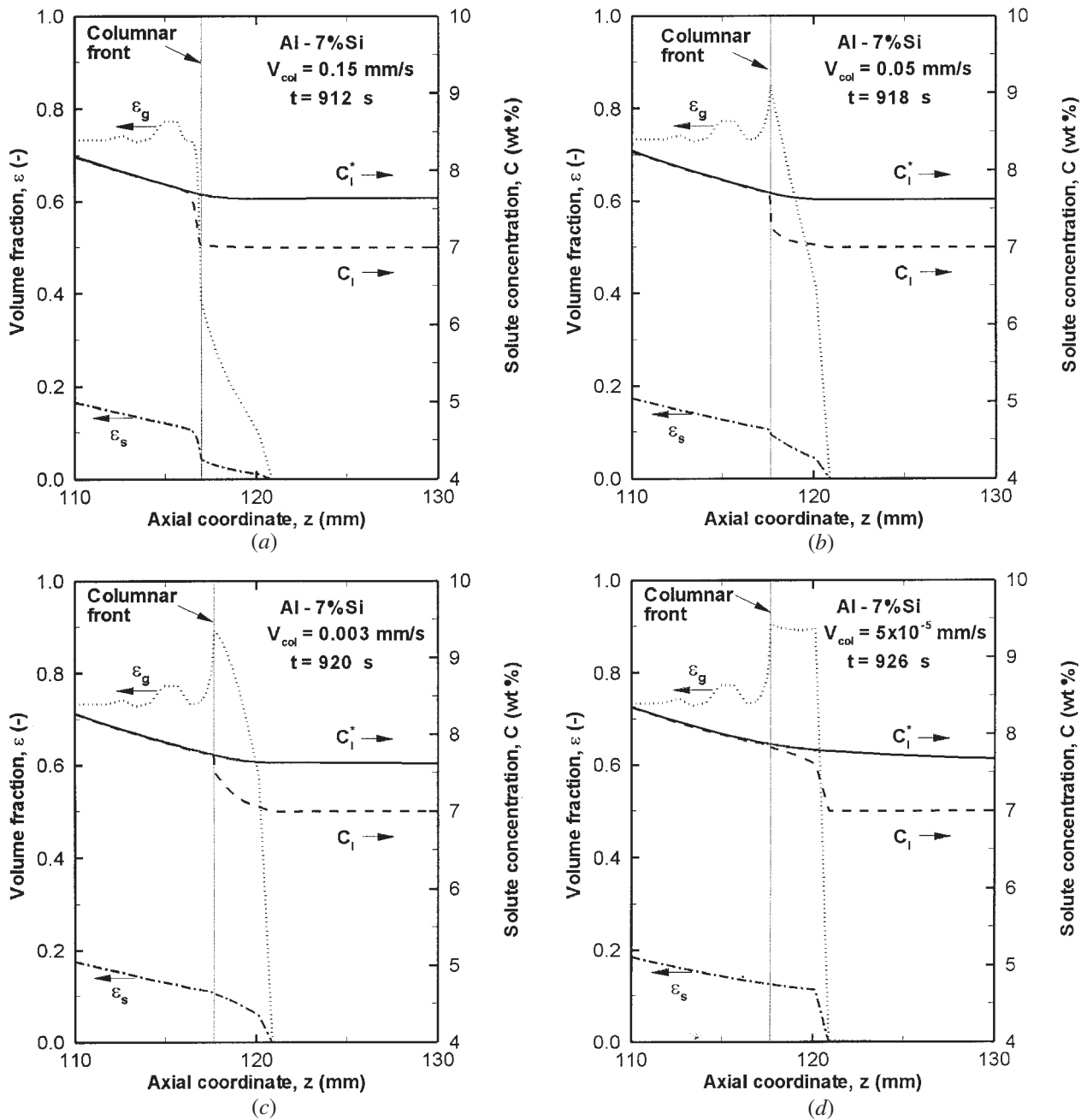
Fig. 11—Predicted volume fraction and solute concentration profiles near the CET in the Al-7 pct Si experiment: (*a*) 912 s, (*b*) 918 s, (*c*) 920 s, and (*d*) 926 s.

would predict a fully equiaxed structure, whereas the Hunt-LGK model would result in a CET at 80 mm, assuming a constant equiaxed grain density.

F. *Discussion*

The key finding from the aforementioned match of the predictions with the Al-Si experiments of Gandin[21] is that for each of the three alloy compositions, the nucleation undercooling for the equiaxed grains is about equal to (but slightly smaller than) the maximum columnar tip undercooling, as previously deduced by Gandin.[20] This finding is insensitive to the equiaxed grain density. Furthermore, the CET is predicted to occur very abruptly and is caused by solutal

interactions with equiaxed grains that exist in a layer ahead of the columnar front, which is slightly thicker than the final equiaxed grain radii.

Thus, the main question remaining is why the nucleation undercooling varies with composition in the manner depicted in Figure 10, *i.e.*, a more than twofold increase (from 2.6 to 5.9 K) for C_0 increasing from 3 to 11 pct. Only if this variation of ΔT_N with C_0 could be obtained from a separate nucleation model would the CET model be of a truly predictive nature.

It is unlikely that any heterogeneous nucleation model would predict that ΔT_N is close to the maximum columnar front undercooling in all three Al-Si experiments of Gandin.[21] Therefore, the origin of the equiaxed grains in these
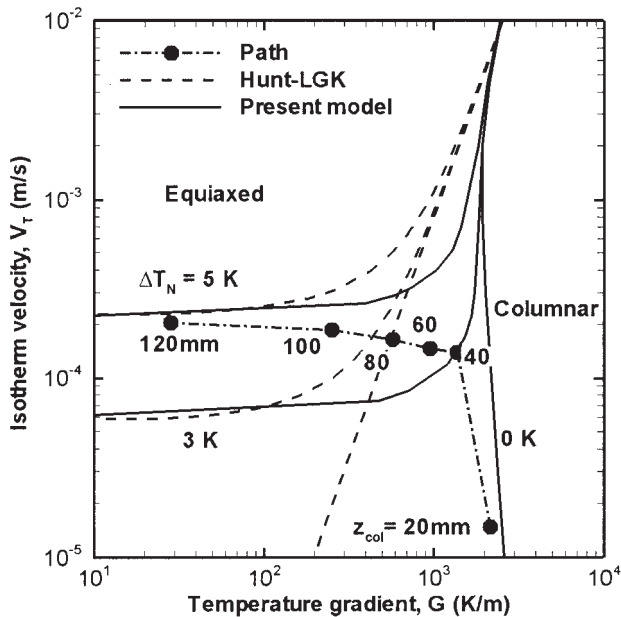
Fig. 12—CET map for the Al-7 pct Si experiment; the solidification path is indicated as a solid line with solid circles that indicate the position of the columnar front.

experiments might not be heterogeneous nucleation ahead of the columnar front, but breakdown or fragmentation of the columnar dendrites, as proposed by Gandin.[20] Jackson *et al.*[22] first observed that a decrease in the columnar front velocity caused dendrite arm remelting and fragmentation. In fact, the model results of Gandin[20] showed that, if the columnar front had not been blocked by equiaxed grains, its velocity would have reached a maximum approximately at the CET position, establishing conditions for dendrite arm remelting and fragmentation. Afterward, convection could have transported fragments to regions ahead of the columnar front. The near-zero thermal gradient in the liquid would prevent the fragments from remelting. Thus, such a fragmentation scenario would lead to a simple CET criterion based on the position of the maximum columnar front velocity (or maximum ΔT_t).

The present model considers nucleation ahead of the columnar front as the only mechanism for equiaxed grain formation. However, as suggested by Gandin,[20] the effect of fragmentation could be simulated by assuming that nucleation occurs when fragments form, *i.e.*, by setting ΔT_N close to the maximum ΔT_t, which corresponds to the maximum columnar front velocity. However, this has to be done by iteration, as in Section IV–C, since the maximum ΔT_t value is not known beforehand in transient directional solidification. Alternatively, a model of fragmentation would need to be developed and incorporated in the present model.

V. CONCLUSIONS

The multiphase/multiscale model of Wang and Beckermann[14] has been applied to study the CET in alloy solidification. The main new feature introduced in the model is the concept of solutal blocking of the columnar front, which

should be opposed to a mechanical blocking criterion based on a critical equiaxed grain fraction, as introduced by Hunt.[6] The solute blocking effect is achieved in the model by basing the undercooling that drives dendrite tip growth on the average solute concentration of the liquid surrounding the grain envelopes (extradendritic liquid), instead of the initial alloy composition. When the solute rejected from the equiaxed grains is sufficient to dissipate the undercooling at the columnar front (such that C_l has increased to C_l^*), the CET will occur.

The model is first examined in a parametric study for simple quasi-steady solidification systems and is compared to the model of Hunt.[6] In the limit of small thermal gradients or large isotherm velocities, the present model gives CET predictions similar to those from Hunt's model, if the same dendrite tip growth model is used. For intermediate G and V_T values, considerable differences become apparent as the equiaxed grain density increases. This is a result of different intensities of solute rejection from the grains, which is predicted by the present model, but not considered in Hunt's model.[6] In particular, for inoculated melts with a globulitic equiaxed-grain morphology, the CET can occur at equiaxed grain fractions well below 0.5.

The present model is validated by simulating the Al-Si experiments of Gandin[21] for three different alloy compositions. Good agreement is obtained between the measured and predicted cooling curves. For each alloy composition, it is found that the nucleation undercooling is very close to the maximum columnar dendrite tip undercooling and that the CET is virtually independent of the equiaxed nuclei density. Furthermore, the CET is predicted to occur abruptly, with equiaxed growth taking place only over a small distance ahead of the columnar front, even though the thermal gradient in the liquid is very small. This finding supports the suggestion by Gandin[20] that the origin of the equiaxed grains in his experiments is breakdown or fragmentation of the columnar dendrites, rather than heterogeneous nucleation.

An additional test of the model could be obtained by performing CET experiments with different levels of grain refiner. The grain refiner would reduce the nucleation undercooling, such that the CET would occur at higher thermal gradients (and growth velocities). The effect of grain refinement on the grain structure and the CET in directionally solidified Al-Mg alloys has recently been investigated in detail by Vandyoussefi and Greer.[28] Finally, it would also be useful to perform experiments using transparent model alloys in order to observe the CET mechanism directly.

APPENDIX

Equation [13] for the solute diffusion length, δ_e, at a growing spherical grain envelope is derived by considering the system shown in Figure A1. The domain consists of a spherical unit cell of radius R_f. The dendrite envelope has an instantaneous radius R_e and an outward velocity V, which is given by Eq. [8] and assumed constant. The following one-dimensional solute conservation equation governs diffusion in the spherical extradendritic liquid space between R_e and R_f:

$$\frac{\partial C}{\partial t} = \frac{D_l}{r^2} \frac{\partial}{\partial r}\left(r^2 \frac{\partial C}{\partial r}\right) \qquad [A1]$$

where C is the local (microscopic) solute concentration and r is the radial coordinate. As shown in Figure A1, the concentration profile in the extradendritic liquid can be expected to decrease exponentially ahead of the moving envelope. The concentration at the envelope surface is C_l^* and the average concentration of the extradendritic liquid is C_l.

In order to facilitate an analytical solution, Eq. [A1] is rewritten in a moving reference frame and simplified by assuming a quasi-steady state. This results in

$$\frac{d^2C}{dr^2} + \left(\frac{V}{D_l} + \frac{2}{r}\right)\frac{dC}{dr} = 0 \qquad [A2]$$

Note that for a sufficiently large envelope Peclet number, $Pe = VR_e/D_l$, the interface curvature term (*i.e.*, $2/r$) can be neglected, and Eq. [A2] approaches that for a planar moving interface at steady state. Conversely, for $Pe \ll 1$, Eq. [A2] becomes a spherical diffusion equation for a stationary interface. Equation [A2] was solved subject to the following conditions:

$$C = C_l^* \quad \text{at} \quad r = R_e \qquad [A3]$$

$$C_l = \frac{3}{4\pi\,(R_f^3 - R_e^3)}\int_{R_e}^{R_f} C(4\pi\,r^2)dr \qquad [A4]$$

Equation [A4] is strictly not a boundary condition, but rather enforces that the average solute concentration in the extraden-
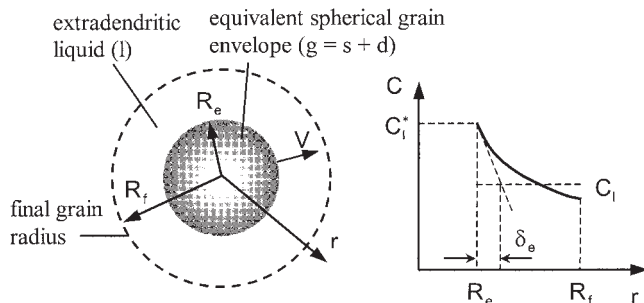
dritic liquid is equal to C_l. This integral constraint is used instead of a zero flux condition at $r = R_f$.

The definition of the envelope diffusion length is given by (Figure A1)

$$\delta_e \equiv \frac{(C_l^* - C_l)}{-\dfrac{\partial C}{\partial r}\bigg|_{R_e}} \qquad [A5]$$

Evaluating the concentration gradient at the envelope surface in Eq. [A5] using the concentration profile resulting from the solution of Eqs. [A2] through [A4] yields for the diffusion length:

$$\frac{\delta_e}{R_e} = \frac{R_e}{(R_f^3 - R_e)}\left[\left(\frac{R_f R_e}{Pe} + \frac{R_e^2}{Pe^2} - R_f^2\right)e^{-Pe\left(\frac{R_f}{R_e}-1\right)}\right.$$

$$- \left(\frac{R_e^2}{Pe} + \frac{R_e^2}{Pe^2} - \frac{R_f^3}{R_e}\right) \qquad [A6]$$

$$\left.+ Pe\frac{R_f^3}{R_e}\left(e^{-Pe\left(\frac{R_{f-1}}{R_e}\right)}\frac{Iv\left(Pe\dfrac{R_f}{R_e}\right)}{Pe\dfrac{R_f}{R_e}} - \frac{Iv(Pe)}{Pe}\right)\right]$$

The use of Eq. [A6] can create numerical difficulties in the limit of $Pe \to 0$, because $Iv(Pe \to 0) \to \infty$. Therefore, for $Pe < 10^{-5}$, the following expression is recommended:

$$\frac{\delta_e}{R_e} = \left(1 - \frac{3}{2}R_e\frac{(R_f^2 - R_e^2)}{(R_f^3 - R_e^3)}\right) \qquad [A7]$$

Equation [A7] is the limit of Eq. [A6] as $Pe \to 0$.

It was verified that, although the expression for the envelope diffusion length derived by Wang and Beckermann[30] is formally different from Eq. [A6], the two give very similar results.

REFERENCES

1. S.C. Flood and J.D. Hunt: *ASM Handbook*, ASM, Materials Park, OH, 1998, vol. 15, pp. 130-36.
2. W.C. Winegard and B. Chalmers: *Trans. ASM*, 1954, vol. 46, pp. 1214-23.
3. J.A. Spittle and S.G.R. Brown: *J. Mater. Sci.*, 1989, vol. 23, pp. 1777-81.
4. P. Zhu and R.W. Smith: *Acta Metall. Mater.*, 1992, vol. 40, pp. 683-92.
5. Ch.-A. Gandin and M. Rappaz: *Acta Mater.*, 1994, vol. 42, pp. 2233-46.
6. J.D. Hunt: *Mater. Sci. Eng.*, 1984, vol. 65, pp. 75-83.
7. S. Kim and R.N. Grugel: *Metall. Trans. A*, 1992, vol. 23A, pp. 1807-15.
8. L.J. Ledgard and D.G. McCartney: *Proc. 4th Decennial Int. Conf. on Solidification Processing*, Sheffield, UK, 1997, pp. 277-80.
9. S.C. Flood and J.D. Hunt: *J. Cryst. Growth*, 1987, vol. 82, pp. 543-51.
10. S.C. Flood and J.D. Hunt: *J. Cryst. Growth*, 1987, vol. 82, pp. 552-60.
11. E. Scheil: *Z. Metallkd.*, 1942, vol. 34, pp. 70-72.
12. M. Gäumann, C. Bezençon, P. Canalis, and W. Kurz: *Acta Mater.*, 2001, vol. 49, pp. 1051-62.
13. W. Kurz, C. Bezençon, and M. Gäumann: *Sci. Technol. Adv. Mater.*, 2001, vol. 2, pp. 185-91.
14. C.Y. Wang and C. Beckermann: *Metall. Mater. Trans. A*, 1994, vol. 25A, pp. 1081-93.
15. J. Lipton, M.E. Glicksman, and W. Kurz: *Mater. Sci. Eng.*, 1984, vol. 65, pp. 57-63.

Fig. A1—Schematic illustration of the unit cell used in the derivation of the expression for the envelope diffusion length.

16. R.B. Mahapatra and F. Weinberg: *Metall. Trans. B*, 1987, vol. 21B, pp. 425-32.
17. I. Ziv and F. Weinberg: *Metall. Trans. B*, 1989, vol. 20B, pp. 731-34.
18. M. Rappaz, X. Doré, Ch.-A. Gandin, A. Jacot, and T. Jalanti: in *Materials Science Forum*, H. Driver, B. Dubost, F. Durand, R. Fougeres, P. Guyot, P. Sainfort, and M. Suery, eds., Trans Tech Publications Ltd., Aedermannsdorf, Switzerland, 1996, vols. 217-222, pp. 7-17.
19. Ch.-A. Gandin, J.-L. Desbiolles, M. Rappaz, and P. Thévoz: *Metall. Mater. Trans. A*, 1999, vol. 30, pp. 3153-65.
20. Ch.-A. Gandin: *Acta Mater.*, 2000, vol. 48, pp. 2483-501.
21. Ch.-A. Gandin: *Iron Steel Inst. Jpn.*, 2000, vol. 40, pp. 971-79.
22. K.A. Jackson, J.D. Hunt, D.R. Uhlmann, and T.P. Seward: *Trans. AIME*, 1966, vol. 236, pp. 149-58.
23. V.K. Suri, N. El-Kaddah, and J.T. Berry: *Trans. AFS*, 1991, vol. 99, pp. 187-91.
24. C.A. Siqueira, N. Cheung, and A. Garcia: *Metall. Mater. Trans. A*, 2002, vol. 33A, pp. 2107-118.
25. M.A. Martorano and J.D.T. Capocchi: *Int. J. Heat Mass Transfer*, 2000, vol. 43, pp. 2541-552.
26. M.A. Martorano and J. D. T. Capocchi: *Int. J. Cast Met. Res.*, 2000, vol. 13, pp. 49-57.
27. A.E. Ares and C. E. Schvezov: *Metall. Mater. Trans. A*, 2000, vol. 31A, pp. 1611-25.
28. M. Vandyoussefi and A.L. Greer: *Acta Mater.*, 2002, vol. 50, pp. 1693-1705.
29. S.V. Patankar: *Numerical Heat Transfer and Fluid Flow*, Hemisphere Publishing Corp., New York, NY, 1980.
30. C.Y. Wang and C. Beckermann: *Metall. Trans. A*, 1993, vol. 24A, pp. 2787-2801.